Exp Fluids (2017) 58:132
DOI 10.1007/s00348-017-2417-8

RESEARCH ARTICLE

Flow around a slotted circular cylinder at various angles of attack

Dong-Lai Gao[1] · Wen-Li Chen[1,2] · Hui Li[1,2] · Hui Hu[3]

Received: 18 March 2017 / Revised: 13 August 2017 / Accepted: 21 August 2017 / Published online: 5 September 2017

Abstract We experimentally investigated the flow characteristics around a circular cylinder with a slot at different angles of attack. The experimental campaign was performed in a wind tunnel at the Reynolds number of $Re = 2.67 \times 10^4$. The cylindrical test model was manufactured with a slot at the slot width $S = 0.075\ D$ (D is the diameter of the cylinder). The angle of attack α was varied from 0° to 90°. In addition to measuring the pressure distributions around the cylinder surface, a digital particle image velocimetry (PIV) system was employed to quantify the wake flow characteristics behind the baseline cylinder (i.e., baseline case of the cylinder without slot) and slotted cylinder at various angles of attack. Measurement results suggested that at low angles of attack, the passive jet flow generated by the slot would work as an effective control scheme to modify the wake flow characteristics and contribute to reducing the drag and suppressing the fluctuating lift. The flip-flop phenomenon was also identified and discussed with the slot at 0° angle of attack. As the angle of attack α became 45°, the effects of the slot were found to be minimal. When the angle of attack α of the slot approached 90°, the self-organized boundary layer suction and blowing were realized. As a result, the flow separations on both sides of the test model were found to be notably delayed, the wake width behind the slotted cylinder was decreased and the vortex formation length was greatly shrunk, in comparison with the baseline case. Instantaneous pressure measurement results revealed that the pressure difference between the two slot ends and the periodically fluctuating pressure distributions would cause the alternative boundary layer suction and blowing at $\alpha = 90°$.

✉ Wen-Li Chen
cwl_80@hit.edu.cn

[1] Key Lab of Smart Prevention and Mitigation of Civil Engineering Disasters of Ministry of Industry and Information Technology, Harbin Institute of Technology, Harbin 150090, China

[2] Key Lab of Structures Dynamic Behavior and Control of Ministry of Education, Harbin Institute of Technology, Harbin 150090, China

[3] Department of Aerospace Engineering, Iowa State University, Ames, IA 50011, USA

1 Introduction

The understanding of flow around a bluff body is of great importance owing to its significance in fundamental fluid mechanics as well as many related engineering applications. A circular cylinder, with a relatively simple shape, is a typical and the most commonly studied bluff body. Flow characteristics, including flow-induced forces acting on the body, flow instabilities, flow patterns and vortex shedding behaviors in the wake of circular cylinder, have attracted extensive research interests. A perspective outlook on bluff body flows in general and flow around a circular cylinder in particular has been contributed by Roshko (1993).

For a circular cylinder immersed in a moving flow, it is characterized with flow separation and periodic vortex shedding downstream in its near wake (Brika and Laneville 1993). If the circular cylinder is free to oscillate, vortex-induced vibrations (VIVs) may take place when its vortex shedding frequency fits some order of the structure's natural frequency. Extensive efforts have been dedicated to develop various passive and active control techniques to manipulate the flow and mitigate the potential VIVs, as reviewed in Choi et al. (2008). Concerning active control, Dong et al. (2008) introduced a novel flow control concept of windward suction and leeward blowing (WSLB) to eliminate the alternating vortex shedding in the wake. By using the WSLB

control, the wake instability was modified and the vortex induced cross-flow vibrations were substantially suppressed. Baek and Karniadakis (2009) extended the WSLB concept and investigated the flow around a circular cylinder geometrically modified with a slot parallel to the incoming flow. The slot was used to form a communicating channel between the windward and leeward stagnation points. The passive WSLB scheme worked as a zero-net-mass flux (ZNMF) actuator. The numerical simulation results suggested that the slot could cause strong jets into the wake flow and interact with the wake vortices behind the cylinder. As a result, the vortex shedding mode was changed and the vortex-induced vibration was effectively suppressed. Wang et al. (2016) successively extended the WSLB concept to both open-loop and closed-loop implementations. They performed a Lattice–Boltzmann method-based numerical study to demonstrate that in the open-loop control, the combination of WSLB was the most effective, while the pure suction was the least. In the closed-loop control, the effects of the four key control parameters, i.e., the proportional gain constant, the integral gain constant, the length of data history used for the feedback and the location of the sensor, were investigated.

In some cases, suppressions on fluidic forces are desired, while in some other particular cases greater fluidic forces are expected. For example, a greater lift force will enhance the flight control of an airplane, and a larger flow-induced vibration will improve the efficiency of energy harvesting. As early as in his first papers in the year 1904, Ludwig Prandtl described some experiments in controlling boundary layers (Schlichting et al. 1979). Classical methods to control boundary layers include motion of the solid wall (Mittal and Kumar 2003; Degani et al. 1998; Chew et al. 1995), accelerating the boundary layer (Piomelli et al. 2000), boundary layer suction (MacManus and Eaton 2000; Antonia et al. 1995) and cooling the wall (Gran et al. 1974). Active suction is a widely used control strategy, especially in the design of aircraft wings. The underlying philosophy of suction control is to evacuate the decelerated fluid particles from the boundary layer before they have a chance to separate. If the decelerated fluids are removed, a new boundary layer will be formed that is capable of withstanding a certain adverse pressure gradient. With proper arrangements of active suction implementations, the separation from a bluff body could be completely eliminated under favorable flow conditions. The laminar flow control of an aircraft using suction has been reviewed by Joslin (1998).

In addition to active methods, extensive efforts have also been made by modifying the geometries of the bluff bodies to reduce the drag, control the vortex shedding and suppress the VIVs. Dimpled surface (Choi et al. 2006; Zhou et al. 2015), helical strake (Zdravkovich 1981), splitter plates (Bearman 1965; Anderson and Szewczyk 1997; Hwang et al. 2003), hemispherical bump (Owen et al. 2001), passive jet (Chen et al. 2015) and segmented and wavy trailing edge (Rodriguez 1991; Tombazis and Bearman 1997) are classic examples of passive flow control methods. It should be noted that the active flow methods are generally more effective and convenient to obtain optimized flow control effectiveness in comparison to the passive ones. However, nearly every active scheme is costly from the implementation standpoint. The biggest advantage of passive flow control is that it can be easily implemented and require no extra energy expenditures to maintain the control process.

In the present study, an experimental investigation was conducted to examine the flow characteristics around a circular cylinder for the test cases with and without passive flow control using a slot along its axis. While the slot width was fixed at 0.075 D in the present study, the flow characteristics around the slotted cylinder at different angles of attack were studied and discussed. It should be mentioned that the slot width was found to have significant effects on the effectiveness of the passive flow control when the angle of attack (AOA) was fixed at 0°, which has already been addressed extensively in the recent work of Gao et al. (2017). By conducting the experimental investigation of the present study, we found that the passive jet flow control and boundary layer control could be successively achieved by simply changing the angle of attack. In the context that follows, the test model setup and experimental details are introduced in Sect. 2, and the experiment results are presented and discussed in Sect. 3, followed by the conclusion in Sect. 4.

2 Test model and experimental setup

The experimental study was conducted in a low-speed circuit wind tunnel (SMC-WT1) affiliated to the Joint Laboratory of Wind Tunnel and Wave Flume, Harbin Institute of Technology, P. R. China. The wind tunnel has a test section with optical walls and its dimension is 505 mm × 505 mm. With honeycombs and mesh structures mounted upstream, a contraction section was installed ahead of the test section to provide uniform airflow into the test section. Based on the measurement results using a hotwire anemometer probe, the turbulence intensity level in the test section of the wind tunnel was measured to be about 0.36%.

2.1 The slotted circular cylinder

Figure 1a sketches the slotted cylinder model used in the present study. The test model was made of a smooth aluminum alloy cylinder with its outer diameter 50.0 mm. To adapt to the width of the wind tunnel test section, the spanwise length of the test model, L, was determined to be 503.5 mm. With a longitudinal length L_0 of 400.0 mm, a slot was manufactured

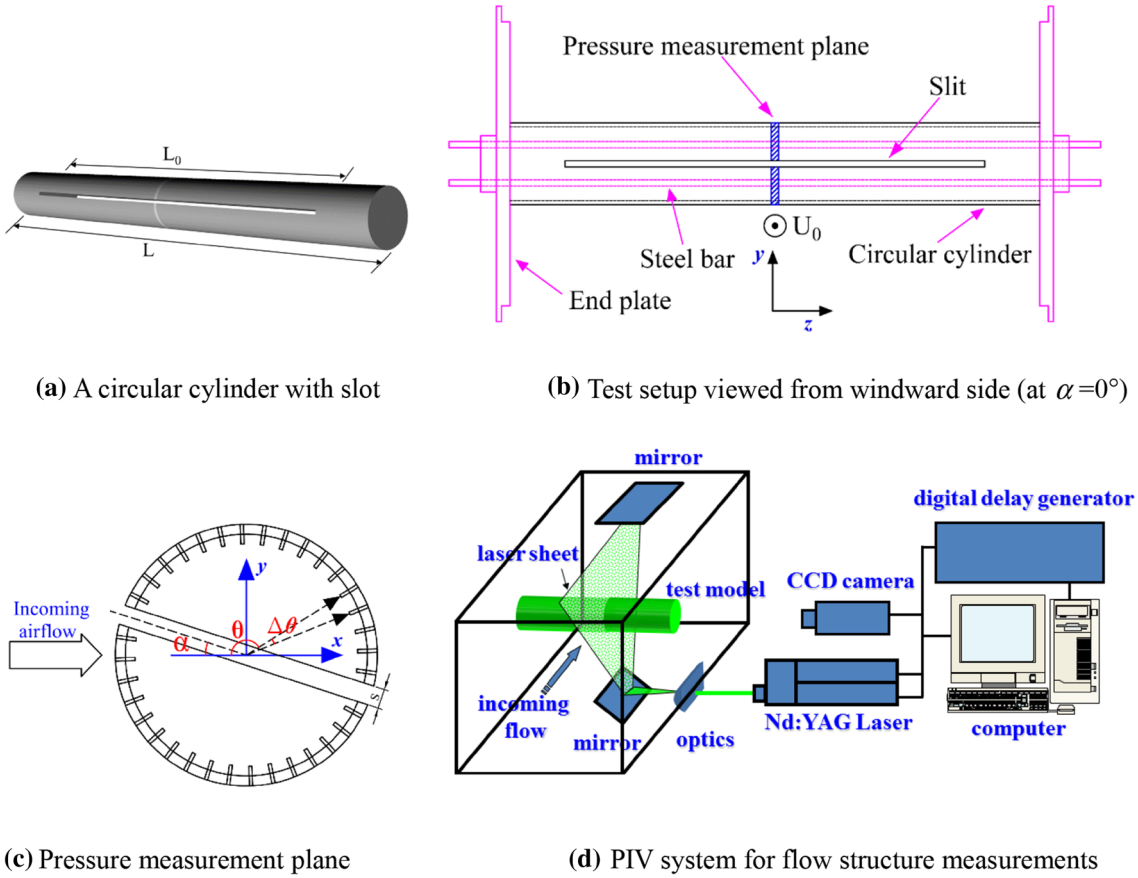

(a) A circular cylinder with slot

(b) Test setup viewed from windward side (at α=0°)

(c) Pressure measurement plane

(d) PIV system for flow structure measurements

Fig. 1 Sketch of the cylindrical model and experimental setup

inside the cylindrical test model. To minimize the errors of the mechanical process, the slotted cylindrical model was manufactured using the computer numerical control (CNC) technique. The width of the slot (S) was set to be 3.75 mm, resulting in a slot ratio (S/D) of 0.075. The value of L_0/S was found to be 106.67; thus, the two-dimensionality of flow around the slotted cylinder was expected in the mid-span. Using two steel bars, the test model was fixed horizontally in the test section of the wind tunnel and was perpendicular to the incoming airflow, as shown in Fig. 1b. Further information about the test model and experimental setup is available in Gao et al. (2017).

As shown in Fig. 1c, the angle of attack, α, of the slot is defined as the angle from the slot center axis to the incoming airflow (i.e., x-axis). During the experiments, α was changed from 0° to 90° with an increment of 15°. For the test case with $\alpha = 0°$, the slot was parallel to the incoming airflow. The slot would be normal to the airflow if α increased to 90°. In addition to the slotted cylinder, a cylinder model without slot was also investigated as the baseline case for the comparative study. During the experimental campaign, the speed of the incoming airflow U_0 was set constant at 8.0 m/s, corresponding to a Reynolds number of $Re = 2.67 \times 10^4$.

2.2 Surface pressure distribution measurement

A digital pressure measurement system, which consisted of three models (DSA3217; Scanivalve Corporation, Liberty Lake, Washington), was employed to measure and record the surface pressure distributions at the mid-span of the cylindrical test model. The pressure measurement plane was made of powdered photosensitive resin and manufactured using a 3D printer. 36 pressure taps were evenly distributed on the pressure measurement plane, i.e., one pressure tap for every 10°. With a sampling rate of 312.5 Hz, the data acquisition time for instantaneous surface pressure measurements was set to be 32 s during the experiments. 36 independent polyvinyl chloride (PVC) tubes with 0.45 m length and 0.9 mm internal diameter were used to connect the pressure taps to the pressure transducer arrays. Based on the findings described in Irwin et al. (1979), the effects of the tubing system, i.e., the signal phase lag and the amplitude attenuation caused by the 0.9-mm-diameter and 0.45-m-long PVC tubing on the instantaneous pressure measurements were expected to be minimal. However, the solid blockage and the wake blockage effects (the blockage ratio is 9.9%) of the test model on the pressure measurements were corrected, as suggested by

Barlow et al. (1999). Some important aerodynamic features (e.g., the lift and drag forces) acting on the test model could be estimated by integrating the measured surface pressure distributions. As suggested in Chen et al. (2014, 2015), the instantaneous lift and drag coefficients acting on the cylinder, C_L and C_D, could be calculated as:

$$C_D = \frac{1}{2}\sum_{\mathrm{i}} C_{p_\mathrm{i}} \cdot \Delta\theta_\mathrm{i} \cdot \cos\theta_\mathrm{i},$$
$$C_L = \frac{1}{2}\sum_{\mathrm{i}} C_{p_\mathrm{i}} \cdot \Delta\theta_\mathrm{i} \cdot \sin\theta_\mathrm{i}, \quad (1)$$
$$C_{p_\mathrm{i}} = \frac{p_i - p_\infty}{\frac{1}{2}\rho U_0^2},$$

where C_{p_i} is the instantaneous pressure coefficient on the model surface, p_i is the static pressure on the test model and p_∞ is the static pressure of the incoming air. The time series of p_i and p_∞ are obtained and recorded by the digital pressure measurement system. θ_i is the azimuthal angle of the pressure tap, and $\Delta\theta_\mathrm{i}$ is the angle difference between the two neighboring pressure taps for the present study, $\Delta\theta_\mathrm{i} = 10°$.

2.3 PIV measurement

In addition to measuring pressure distribution around the surface of the test model, a digital particle image velocimetry (PIV) system was also used to quantify the flow characteristics around the baseline and slotted circular cylinders. Figure 1d shows the schematic of the system setup for the PIV measurements. The vertical plane in the mid-span of the test model was illuminated by a double-pulsed Nd:YAG laser with a repetition rate of 8 Hz. The laser beam was manipulated by a set of optics and mirrors to a thin sheet with a thickness of about 1.0 mm in the target plane. For each test case, 500 frames of instantaneous PIV image pairs were obtained. After acquiring the PIV images, instantaneous velocity vectors were induced using frame to frame cross-correlation technique involving successive frames of the patterns of particle images. The size of the interrogation window was 32 × 32 pixels and an effective overlap of 50% of the interrogation windows was employed in the PIV image processing. After determining the instantaneous velocity vectors (u, v), the instantaneous spanwise vorticity (ω_z) could be derived. The distributions of ensemble-averaged flow quantities, such as the mean velocity (U, V) and in-plane turbulence kinetic energy (T.K.E $= 0.5 \times (\overline{u'^2} + \overline{v'^2})/U_0^2$), could also be obtained from the instantaneous PIV measurements. For the PIV measurements conducted in the present study, the uncertainty level in the velocity measurement was estimated to be within 2.0%, while the measurement uncertainties for the ensemble-averaged flow quantities were about 5%.

3 Experimental results

3.1 Flow characteristics

Derived from the pressure measurement results, Fig. 2 illustrates the mean and fluctuating pressure distributions of the natural and the slotted cylinder at different angles of attack. At low angles of attack, i.e., $\alpha \leq 30°$, the base pressure regions of mean pressure distributions on the leeward side of the slotted cylinders in Fig. 2 were found to be lifted, in comparison to the baseline case (i.e., the surface pressure distribution around the cylinder without slot). This

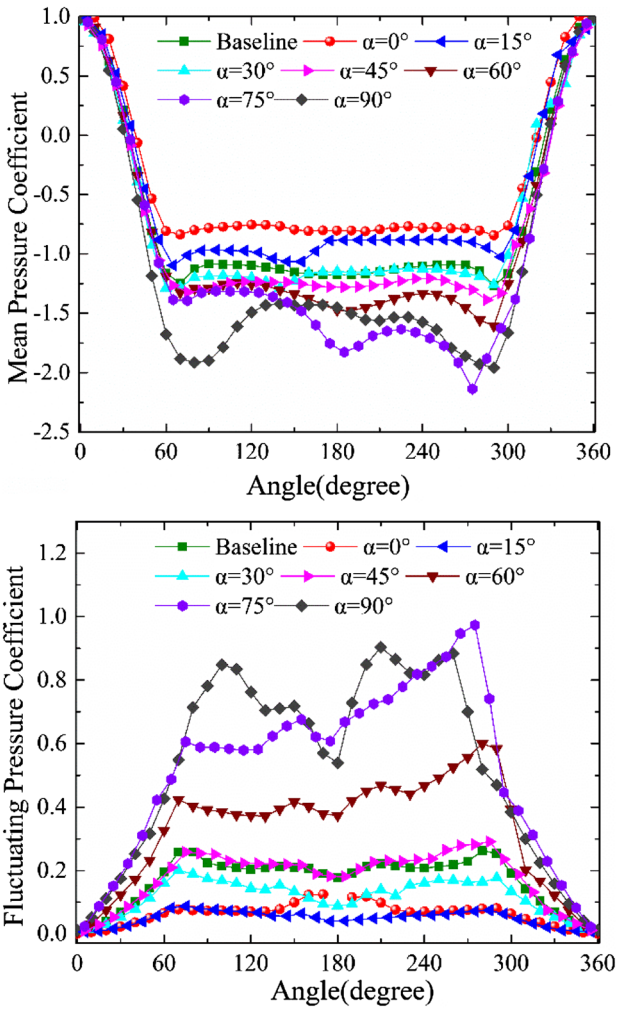

Fig. 2 Mean and fluctuating pressure distributions around the cylindrical models

indicated a drag reduction for the slotted cylinder at low angles of attack. When the angle of attack α changed from 30° to 45°, the base pressure region dropped below that of the baseline case. As the angle of attack α continued to increase, the negative pressure region experienced a remarkable decrease, indicating large drag coefficients for those test cases. According to the distributions of the negative pressure regions, it could also be noted that the separation points were delayed in comparison with the baseline case for the cylinder without slot.

In addition, the root-mean-squared (RMS) values of the instantaneous pressure coefficients were also calculated and presented in Fig. 2 to quantify the fluctuation amplitudes of the pressure distributions around the circular cylinder. It was found that the pressure fluctuation amplitudes were reduced greatly on the leeward side of the slotted cylinder for the test cases with the slot at low angles of attack, indicating a suppression of the unsteady lift forces acting on the cylinder model. When the angle of attack α shifted to 45°, the fluctuating pressure distribution on the slotted cylinder was found to be in good agreement with that of the baseline case. As the angle of attack α continued to increase, the fluctuating pressure distributions on the cylinder surface were found to be quite high, implying that the fluctuating lift forces acting on the cylinder model would become substantially larger.

Based on the pressure measurement results, the mean drag coefficients $\overline{C_D}$, the mean lift coefficients $\overline{C_L}$ and the root-mean-square (RMS) values of the instantaneous lift coefficients C_L' for test cases with different angles of attack were calculated and the results are illustrated in Fig. 3. The dashed lines represented the baseline values measured from the cylinder model without slot. The mean drag coefficient $\overline{C_D}$ for the baseline case was found to be 1.19, and the RMS

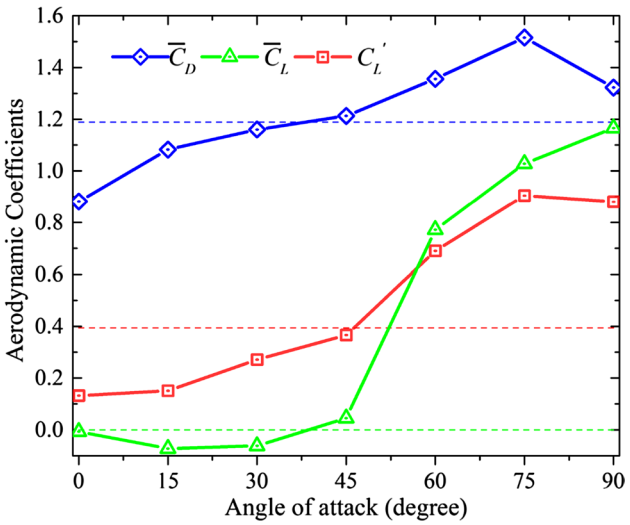

Fig. 3 Aerodynamic coefficients estimated from pressure measurement results

lift coefficient C_L' was 0.39. It was shown clearly that, for the test case with the slot at low angles of attack, both $\overline{C_D}$ and C_L' of the slotted cylinder were clearly decreased, in comparison to the baseline case, suggesting that the slot would work as an effective flow control scheme for drag reduction and lift suppression. Particularly, for the test case with α being set as 0°, a drag reduction of 25.7% and lift suppression of 63.4% were achieved. Therefore, an effective flow control could be achieved by simply manufacturing a slot parallel to the incoming flow. Similar findings were also reported by the previous numerical study of Baek and Karniadakis (2009), who investigated the flow around a circular cylinder with a slot parallel to the incoming flow. The slot was used to form a communicating channel between the windward and leeward stagnation points. In addition, the aerodynamic coefficients of the slotted cylinder were found to be very much close to the baseline values as the angle of attack α increased to 45°. With such a setting, the effects of the slot were expected to be minimal. This finding will be confirmed by PIV measurements to be discussed in the following sections. Furthermore, when the angle of attack α became even higher, the aerodynamic coefficients were found to experience an upward trend. During the experiments, the peak values for the mean drag and RMS of lift coefficients (i.e., $\overline{C_D}$ and C_L') were both found to be at $\alpha = 75°$. For the case, the mean drag coefficient was 27.7% higher than the baseline value, while the RMS of the lift coefficient C_L' was found to be 3.04 times the baseline value. It is also noteworthy that when the angle of attack α was further increased from 75° to 90°, the mean drag coefficient $\overline{C_D}$ would drop remarkably, but was still found to be 11.5% higher than the baseline case. Meanwhile, the RMS value of lift coefficients remained quite high, which was still about 3.01 times the baseline value. It could also be noted that the time-averaged lift coefficient $\overline{C_L}$ for the slotted cylinder would witness a remarkable climb as the angle of attack exceeded 45°, while $\overline{C_L}$ remained 3–5% above or below zero when the angle of attack was in the range of 0°–45°. The maximum $\overline{C_L}$ value was found to be 1.16, which was achieved for the test case at the angle of attack of 90°.

As described above, a high-resolution digital PIV system was employed in the present study to get an insight into the flow characteristics around the slotted circular cylinder at different angles of attack. Following up the work of Sirovich (1987) and Meyer et al. (2007), a method of snapshot proper orthogonal decomposition (i.e., 'snapshot POD') was adopted in the present study for the post-processing of the PIV measurement results.

Figure 4 illustrates the time-averaged flow structures in the mid-span of the test model for different test cases. It was shown that a large recirculation region was formed in the wake behind the natural cylinder without slot (i.e., the

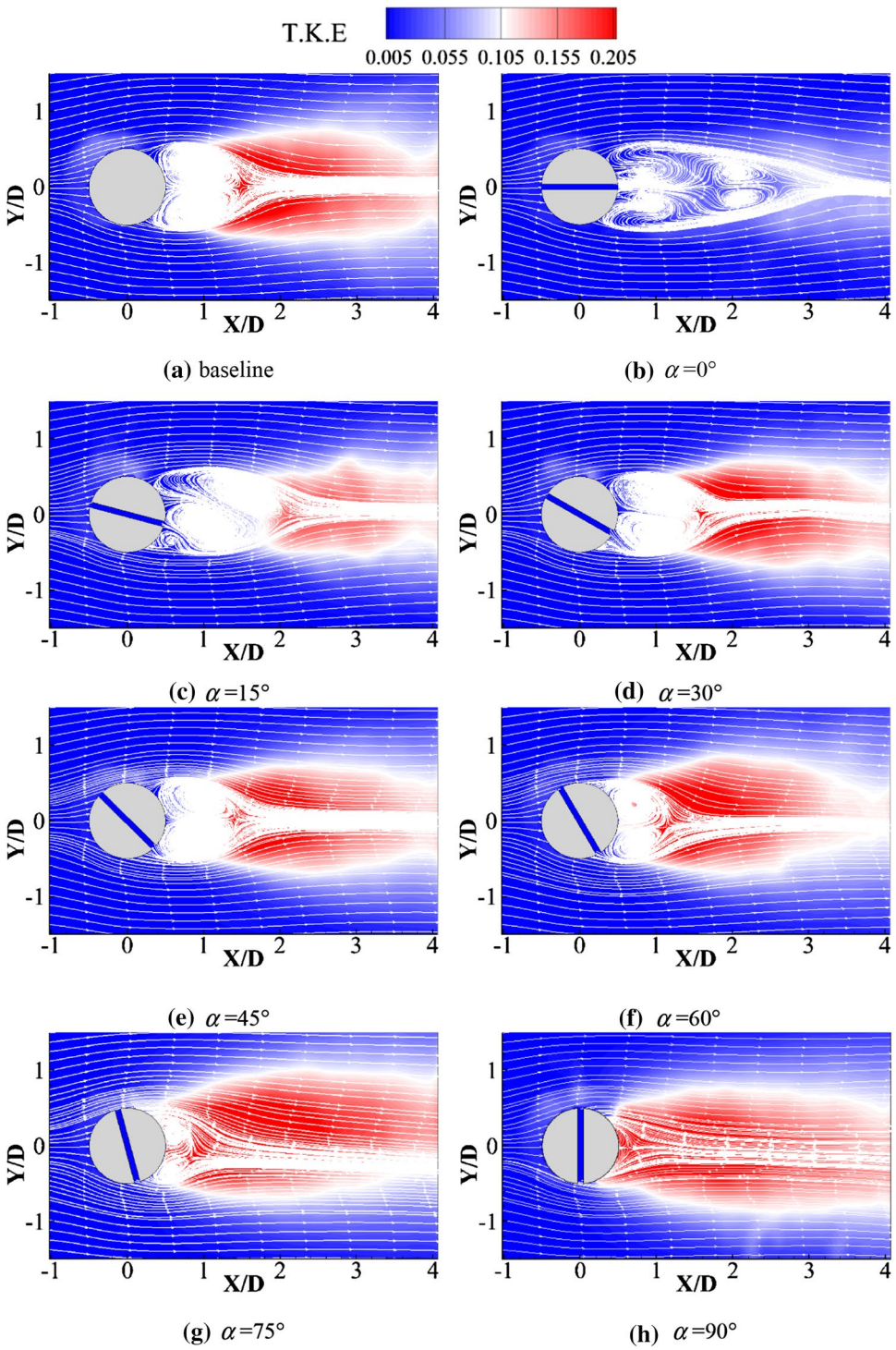

Fig. 4 The time-averaged PIV measurement results in the mid-span plane

baseline case). Besides, the turbulent kinetic energy (TKE) values in the wake of the natural cylinder were found to be quite high, especially along the vortex shedding paths. As suggested by Benard et al. (2008) and Chen et al. (2014, 2015), the TKE values could be used as a measure of the turbulence mixing in the wake flow as well as an indicator to assess the unsteady surface pressures and the fluctuating amplitude of the resultant dynamic wind loads acting on the cylinder. For the slotted cylinder with the slot at the angle of attack $\alpha = 0°$, it could be observed from the time-averaged streamlines that the passive flow would jet into the near wake through the orifice slotted at the leeward stagnation point and interact with the recirculating flow behind the cylinder. The interaction and competition between the jet

flow and the separation flows resulted in two recirculation regions, i.e., an upstream one and a downstream one, in the wake behind the test models. The TKE distributions in the wake flow were found to be substantially decreased, implying that the unsteadiness of the surface pressure and the fluctuating amplitude of the resultant dynamic wind loads acting on the test model were greatly suppressed. In consequence, a drag reduction and lift suppression were achieved, as shown in Figs. 2 and 3. When the angle of attack α of the slot shifted to 15° and 30°, the interactions between the inclined jet flow and the separation flow were found to be weakened. As a result, the Kármán vortex street would form again, and the regions with higher TKE values also became noticeable. Therefore, the effectiveness of the flow control for the passive jet was found to be degraded. At the angle of attack $\alpha = 45°$, the time-averaged flow characteristics, including streamlines, vortex formation length, wake width and TKE distributions, around the slotted cylinder were found to have considerable similarity to those of the natural cylinder. This verified our previously proposed observation, i.e., the effects of the slot would become almost minimized at this angle of attack. When the angle of attack α continued to increase, the vortex formation length witnessed a gradual shrinkage toward the rear surface of the cylinder model and the TKE distributions were found to be gradually strengthened. When the slot was normal to the flow direction, the vortex formation length was found to be greatly shrunk and the flow separation apparently delayed. The boundary layer suction and blowing were realized at the angle of attack $\alpha = 90°$. Due to the boundary layer suction and blowing, the drag and lift coefficients were found to be enhanced, in comparison to the baseline values. A detailed discussion on the boundary layer suction and blowing will be given in Sect. 3.4.

The instantaneous vorticity distributions in the wake flow behind the cylindrical test model for different test cases obtained by the PIV measurement system are presented in Fig. 5. As shown in Fig. 5a, a pair of anti-symmetric vortex structures were found to shed from each side of the cylinder model to form Kármán vortex streets in the wake behind the natural cylinder. For the slotted cylinder at the angle of attack $\alpha = 0°$, a pair of symmetric jet vortices was generated in the near wake behind the cylindrical test model to elongate the shear layers rolled up from both sides of the cylinder model, which helped to detach the alternating vortex street. As a result, the vortex formation region was pushed further downstream. This was believed to be the underlying flow control mechanism for the slotted cylinder at the low angles of attack. With the increase of the angle of attack α for the slot, the interactions between the inclined jet vortices and the separation flow were gradually weakened.

At the angle of attack $\alpha = 45°$, though a weak jet flow still had a chance to form, the jet vortices could hardly be identified in the cylinder wake under this test condition and the resultant wake flow pattern was found to be very similar to that behind the natural cylinder (i.e., baseline case) given in Fig. 5a. As shown in Figs. 2 and 3, the pressure distributions and aerodynamic coefficients for this test case were found to be almost the same as the baseline case. Therefore, it was speculated that the effectiveness of flow control with the slot would be the minimal at $\alpha = 45°$.

As the angle of attack α changed from 60° to 90°, there existed a vortex adhering to the suction side of the cylinder surface, while a strong vortex rotating in an opposite direction was formed on the other side. As the vortex was shed into the wake flow, the blowing side would convert to be the suction side. Consequently, the boundary layer suction and blowing were found to appear alternatively and a vortex street was formed behind the slotted cylinder. It is also noticeable in Fig. 5 that, with the increase of angle of attack α for the slot, the vortex formation length would witness a gradual shrinkage and the strength of the vortices was gradually enhanced.

Based on the pressure measurement and PIV measurement results described above, it can be concluded that, at low angles of attack ($\alpha = 0°$–$30°$), the slot would contribute to a passive jet flow control, while the effects of the slot were found to become almost negligible with the angle of attack of the slot reaching 45°. Furthermore, when the angle of attack of the slot varied from 60° to 90°, the boundary layer suction and blowing were found to take place. To gain further insight into the process and mechanism of the passive jet and boundary layer suction and blowing, a more detailed flow measurement was also conducted using the digital PIV system.

3.2 Passive jet and flip-flop at $\alpha = 0°$

Figure 6 shows the time-averaged streamlines behind the slotted cylinder obtained based on 500 frames of instantaneous PIV measurements. It revealed clearly that, when the jet flow was generated by the slot and evacuated into the wake flow, it competed with the backward flow and was found to be relocated laterally. Afterward, the passive jet flow would interact with the shear layers and they were transported downstream together. In consequence, there were two pairs of vortices being formed behind the cylindrical test model. This vortex system was different from the vortices patterns generally formed in the wake behind a natural cylinder, as discussed above. Figure 6 gives a more detailed look into the upstream recirculation region. Besides, the detailed instantaneous flow structures behind the slotted cylinder are also presented in Fig. 7. It can be seen clearly that the jet flow was deflected toward the upward side, downward side or streamwise-oriented intermittently. The jet vortices shed from the slot orifice were expected to be small scale and symmetric, while the vortices rolled up from the unstable shear layers

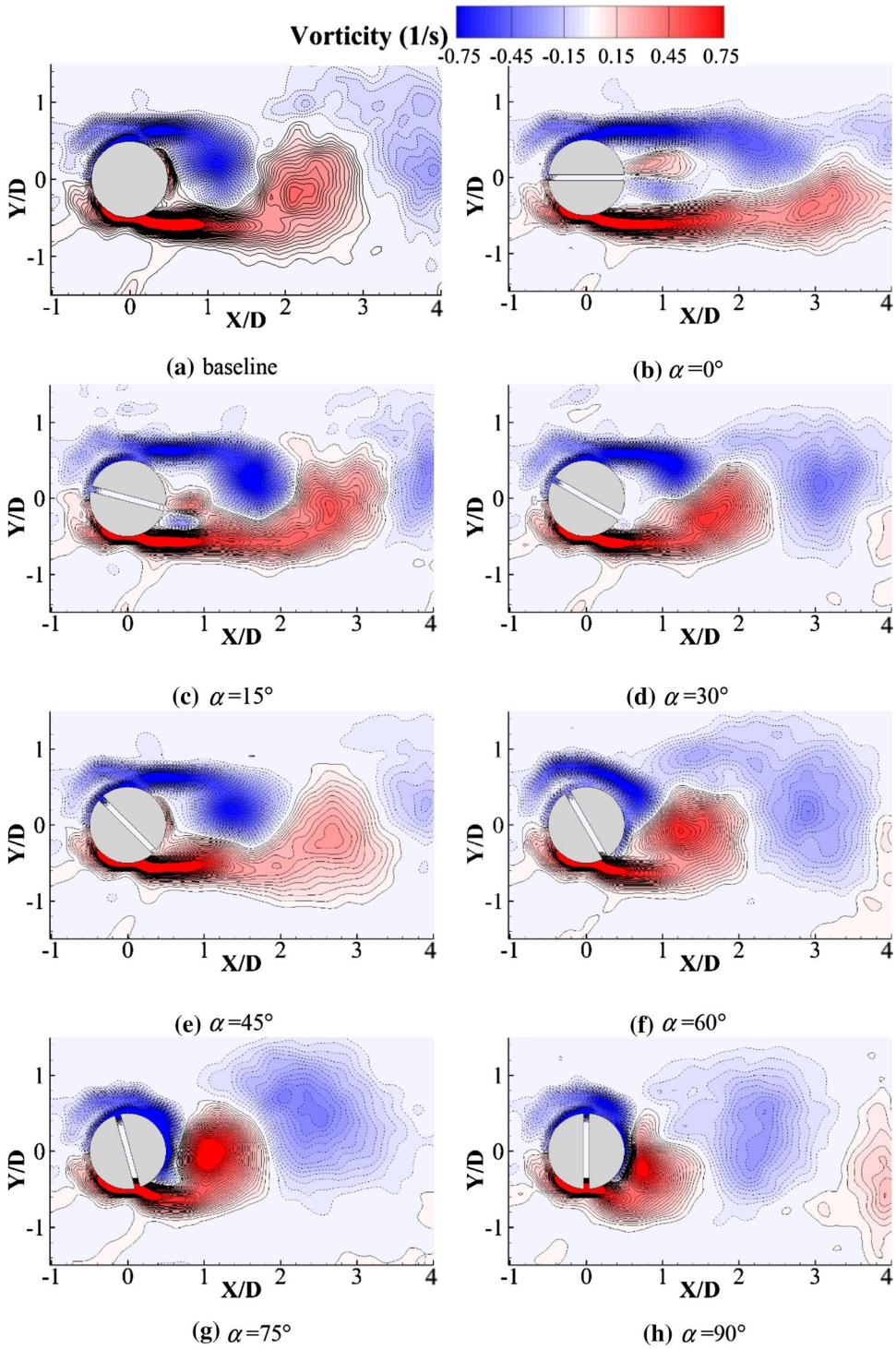

Fig. 5 The instantaneous PIV measurement results in the mid-span plane

of the cylinder were found to be essentially alternating and asymmetric. The competition between the small-scale jet vortices and the asymmetric-mode instability led to the deflected flow patterns in the near wake. This phenomenon, often referred to as flip-flop, is usually found in the coupled wakes of two bluff bodies with a gap (Bearman and Wadcock 1973; Williamson 1985; Kim and Durbin 1988; Zhou et al. 2002). The flip-flop was characterized by an unsteady wake as a result of the gap flow being intermittently deflected toward the upside or downside of the cylinders; therefore, the forces acting on the cylinder were affected by the bistable wake flows. Figure 8a illustrates an arbitrary segment of lift coefficient time history. The blue dashed line denotes the baseline case, while the red solid line represents the

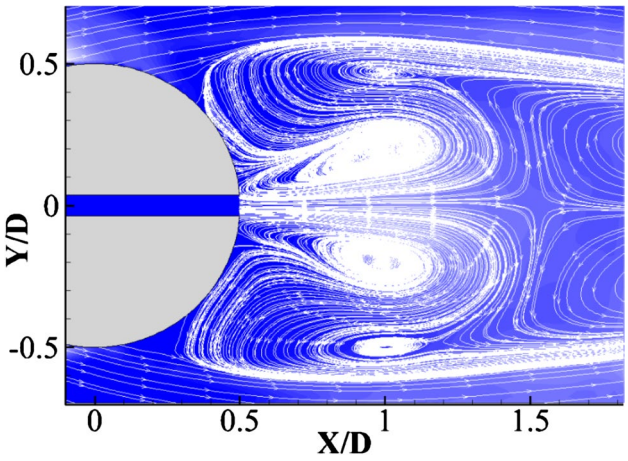

Fig. 6 Time-averaged streamlines in the near wake of the slotted cylinder at $\alpha = 0°$

lift coefficients of the slotted cylinder at α of 0°. It can be seen that the fluctuation amplitudes of the instantaneous lift forces acting on the slotted cylinder were decreased greatly, in comparison with those of the baseline case. To have a detailed look into the change of lift coefficients, a smaller segment of signal was extracted and presented in Fig. 8b. Sudden switchovers in lift coefficient, which was one of the main characteristics of the flip-flop phenomenon, could be clearly observed. Furthermore, Fig. 9 shows the frequency spectra of the measured dynamic lift forces acting on the test models with and without the slot through a fast Fourier transform (FFT) analysis. It can be seen that the frequency of the flip-flop was significantly lower than the vortex shedding frequency of the natural cylinder case. According to the research findings of Kang (2003), the switchover time was one order larger that the vortex shedding, which suggested that the switchover frequency was at least one order lower

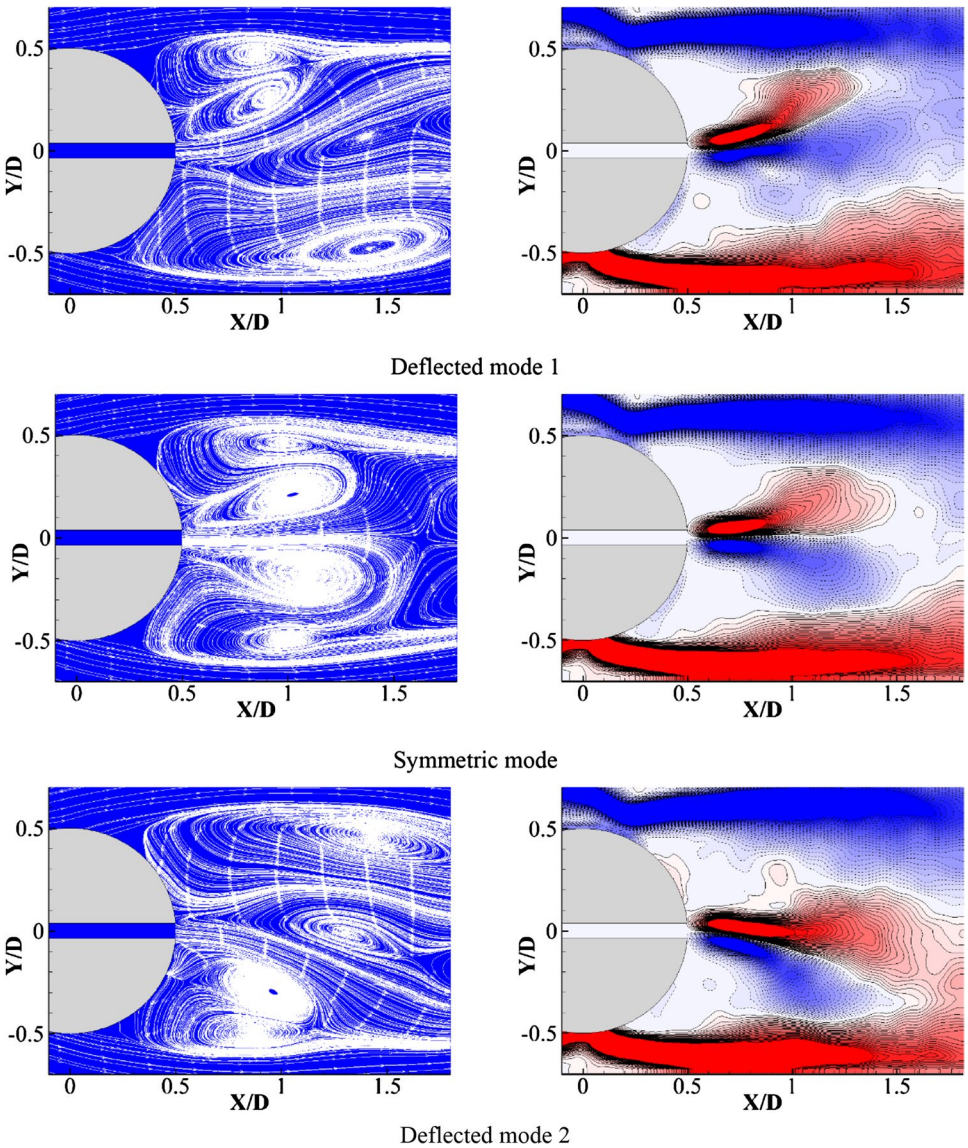

Fig. 7 Bistable flow patterns in the near wake of the slotted cylinder at $\alpha = 0°$

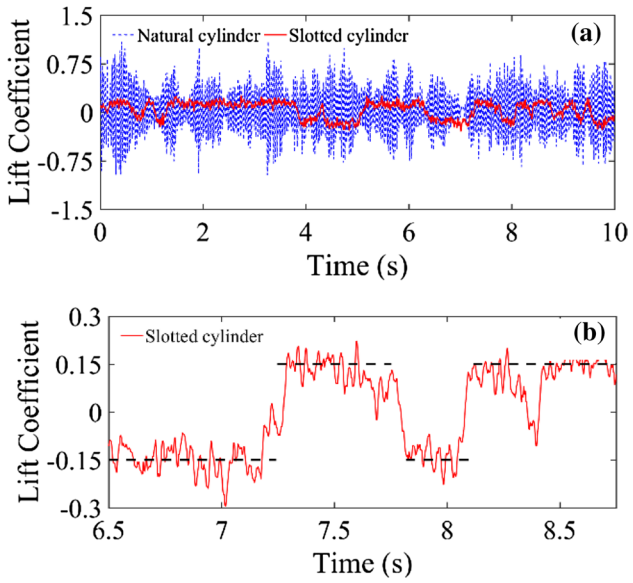

Fig. 8 Time history of the instantaneous lift coefficients

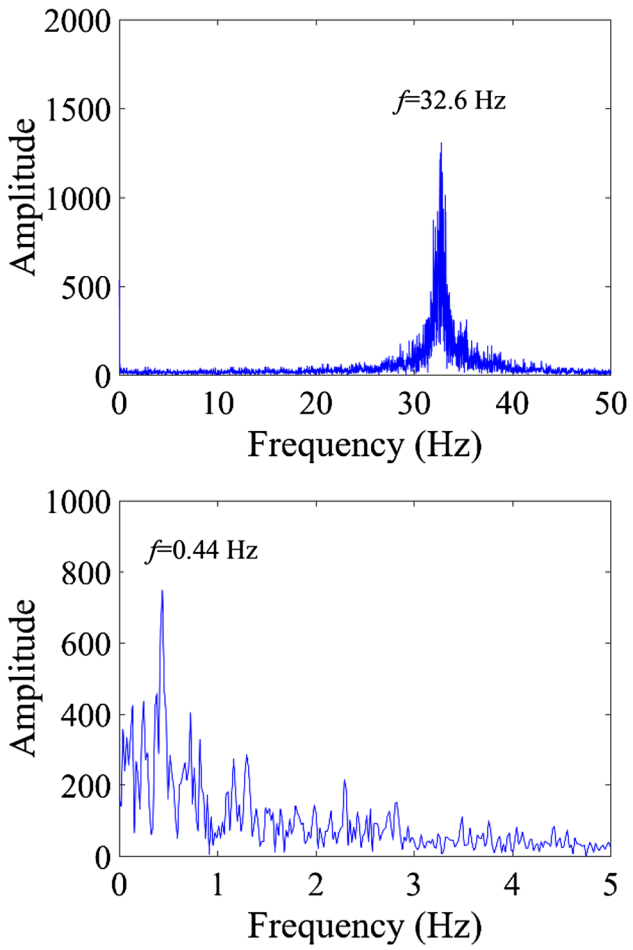

Fig. 9 Frequency spectrum of the lift force time histories: natural cylinder (*up*) and the slotted cylinder at $\alpha = 0°$ (*down*)

than the vortex shedding. Moreover, as reported in many previous studies, one noticeable features of the flip-flop phenomenon was that it consisted of multiple timescales which exhibited little regularity, i.e., the switchover time interval was intermittent and even random. It is worth noting that during our experimental campaign, 12 groups of successive pressure measurements (with a sampling frequency of 312.5 Hz and a sampling time of 32 s for each group) were repeated for each test case. At the angle of attack α of 0°, the switchover frequency in the lift force for each recorded signal was identified to be random, though it remained at a very low level, as illustrated in Fig. 10. This is also consistent with previous research findings.

As shown in Figs. 4b and 6, two vortex systems were found to form in the wake region of the cylinder: one was attached to the rear wall of the cylindrical test model and the other was located downstream. The absolute instability of the wake flow behind the circular cylinder was responsible for the vortex formation behind a stationary cylinder, as suggested by Triantafyllou et al. (1986). By performing a linear stability analysis, the stability nature of the velocity profile in the wake could be determined. Based on the time-averaged velocity profiles obtained by the PIV measurements at different downstream locations, the expansions in Chebyshev polynomials firstly introduced by Orszag (1971) were adopted to solve the inviscid Orr–Sommerfeld equation. The dispersion relation $\omega = \omega(k)$ mapped k_i constant lines on the ω plane at different *X*/*D* average velocity profiles. For different k_i, a group of quadratic maps with similar shape touched at the critical point that had a coordinate of (ω_r, ω_i). The nature of the instability was determined by the imaginary part of the critical part ω_i. As suggested in Triantafyllou

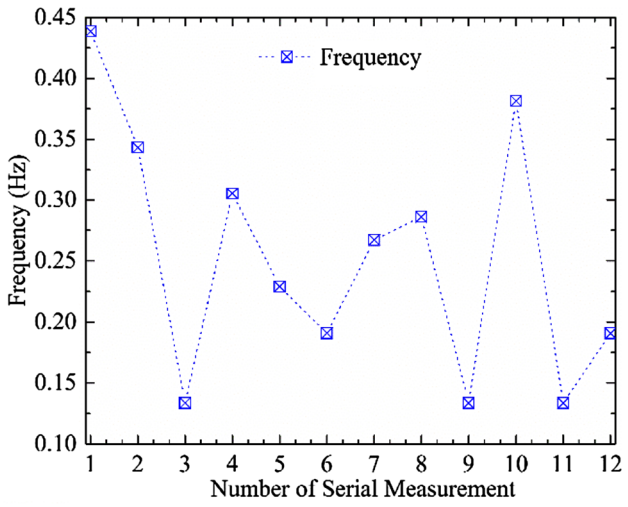

Fig. 10 Frequency variations of the lift time histories for different measurements

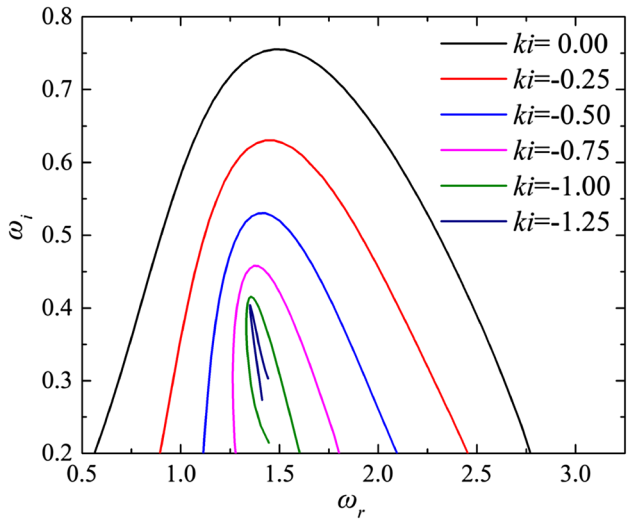

Fig. 11 Map of lines k_i = constant in the ω plane, at $X/D = 0.75$ behind the natural cylinder

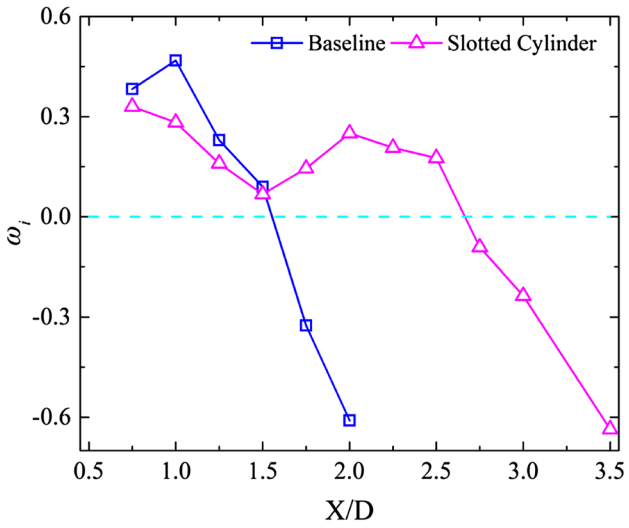

Fig. 12 Imaginary part of the critical point versus X/D for baseline and slotted cylinder

et al. (1986), a positive ω_i supported an absolute instability, while a negative ω_i would support a convective instability.

Figure 11 illustrates a map of iso-value contour lines (i.e., k_i constant) in the complex plane of ω, in which k is the complex wave number and k_i denotes its imaginary part. The Orr–Sommerfeld equation was solved to plot Fig. 11 based on the time-averaged velocity profile behind the natural cylinder at the downstream location of $X/D = 0.75$. The mapped curves touched at the critical point, which looked like a cusp on the plane. As can be identified from Fig. 11, the imaginary part of the critical point was 0.40, while its real part (ω_r) was 1.33. Therefore, the mean velocity profile of the wake flow behind the natural cylinder at the downstream location of $X/D = 0.75$ supported an absolute instability, resulting in the formation of vortex in the near wake. In addition, the Strouhal number (St) could be obtained by the real part of the critical value ω_r, by $\mathrm{St} = \omega_r/2\pi = 0.21$, which was in excellent agreement with the non-dimensional vortex shedding frequency derived from the power spectra analysis of the measured dynamic lift forces acting on the test model (i.e., $\mathrm{St} = fD/U_0 = 0.204$).

Figure 12 illustrates the ω_i values at different downstream locations for the natural and slotted cylinder. It can be seen that with the implementation of a slot, the results of the linear stability analysis showed a great modification in the wake flow. As suggested in Baek and Karniadakis (2009), the local peak values of ω_i predicted the maximum local growth rates, which was associated with the center of vortices formed in the wake. It can be seen from Fig. 4 that the center of the vortices behind the natural cylinder was near the station of $X/D = 1.0$. In Fig. 12, two absolute instability pockets separated by a saddleback valley could be observed in the near wake of the slotted cylinder, which also reflected the evolution of vortex formation. As in Fig. 4, two vortex systems were formed in the wake region: one was attached to the rear surface of the cylindrical test model and the other was located farther downstream. The vortex centers were found close to the location where the predicted peak values of ω_i appeared in Fig. 12.

3.3 Flow structure at $\alpha = 45°$

The time-averaged streamlines around the slotted cylinder at $\alpha = 45°$ are plotted in Fig. 13. It can be seen clearly that only a small amount of airflow was formed and jet into the wake. Besides, the interaction between the jet flow and the separated shear layer near the outflow orifice was weak at this

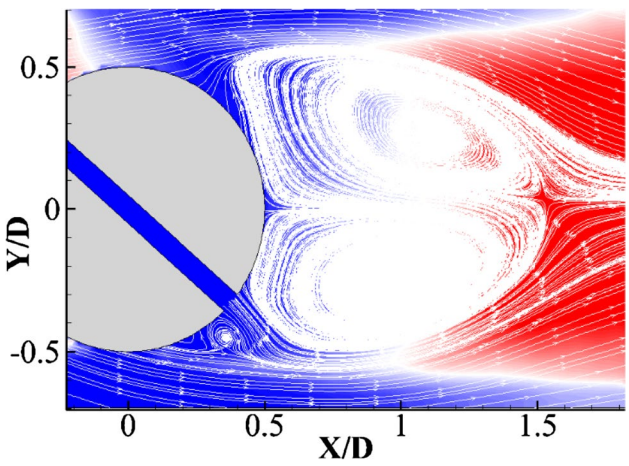

Fig. 13 Time-averaged streamlines in the near wake of the slotted cylinder at $\alpha = 45°$. (TKE contour level is consistent with Fig. 4)

angle of attack. As a result, a symmetric recirculation region was formed in the wake behind the slotted cylinder and the TKE distributions were found to be quite high, which were similar to the flow characteristics around a natural circular cylinder without a slot. Figure 13 confirms that the effects of the slot are almost negligible at the angle of attack $\alpha = 45°$.

3.4 Boundary layer suction and blowing at $\alpha = 90°$

The time-averaged streamlines around the slotted cylinder at $\alpha = 90°$ are plotted in Fig. 14. Due to the boundary layer suction, the low energy fluid in the boundary layer was removed and the flow followed along the surface of the cylinder where the slot was vertically implemented for a considerable distance. As a result, the flow separations on both sides were notably delayed, though not been prevented completely. This observation was consistent with the pressure distributions, as illustrated in Fig. 2. Besides, the wake width behind the slotted cylinder was decreased and the vortex formation length was greatly shrunk in comparison with the natural cylinder. It can be noted that the TKE distributions were not symmetric, despite the symmetry of the model setup and flow conditions. The reason is that the laser sheet was manipulated from the bottom to the upside, and in this case the area near the upper slot could not be sufficiently illuminated by the reflection mirror placed on top, as shown in Fig. 1d.

With respect to the instantaneous flow structures, vorticity analysis as given in the above sections was adopted to identify the dynamic characteristics of vortex motion, including location, size, strength and rotation direction. The objective of the analysis given in this section is to gain an insight into boundary layer suction. However, according to the definition of vorticity, it describes not only the vortex motions but also shearing motions in the flow. In the near-wall region, the strong shear layers will therefore make the identification of the virtual vortices difficult. To identify the vortex structures near the wall more clearly, a concept of swirling strength is adopted in this section. Swirling strength was defined as the imaginary part of the complex eigenvalue of the velocity gradient tensor by Adrian et al. (2000).

The instantaneous swirling strength behind the slotted cylinder at $\alpha = 90°$ was identified and presented in Fig. 15. It can be observed from Fig. 15a that a boundary layer suction was done on the upper end of the slot and the point of flow separation from this side was considerably delayed. A flow that could withstand more adverse pressure gradient was closely adhering to the cylinder wall and was moving along the surface of the suction side. On the other hand, a strong vortex formed and grew at the lower side. Since the slot could be considered as a zero-net-mass flux (ZNMF) actuator, a slot blowing would take place simultaneously at the lower side. In consequence, the shear stress was reduced and the vortex was shed into the near wake. As shown in Fig. 15b, the same phenomenon could be observed, but in

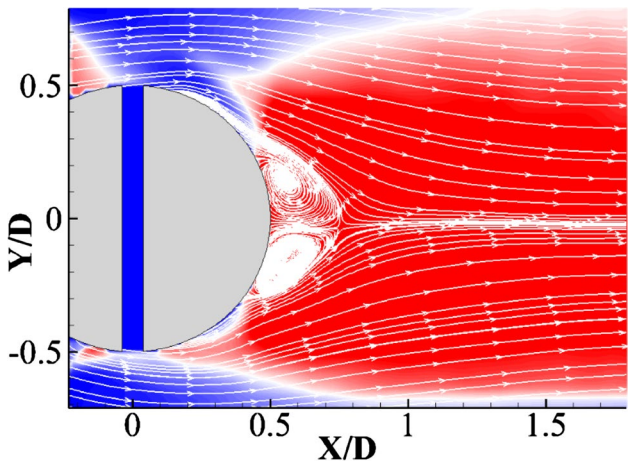

Fig. 14 Time-averaged streamlines in the near wake of the slotted cylinder at $\alpha = 90°$

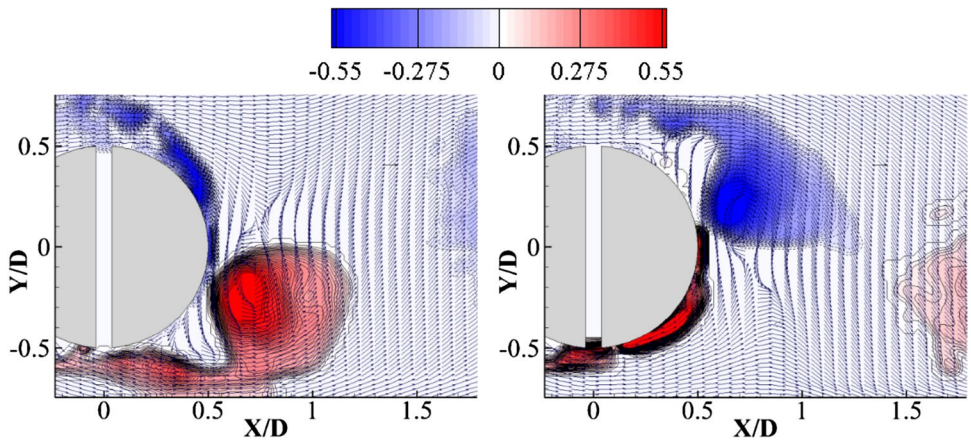

(a) Suction on the upper end (b) Suction on the lower end

Fig. 15 Instantaneous swirling strength in the near wake of the slotted cylinder at $\alpha = 90°$

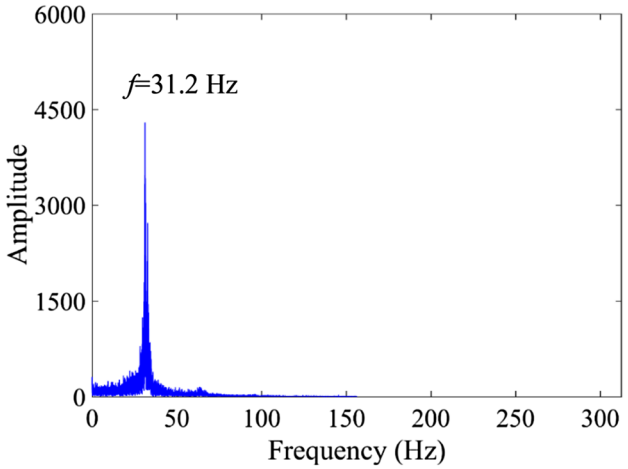

Fig. 16 Frequency spectra of the lift force at $\alpha = 90°$

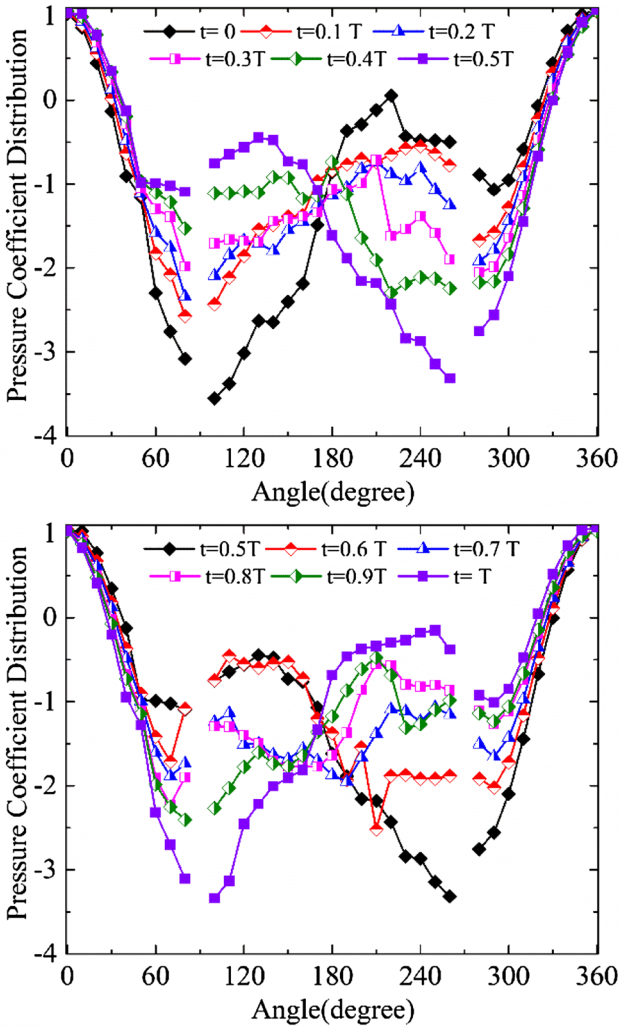

Fig. 17 Instantaneous evolutions of the surface pressure distributions on the slotted cylinder within a period at $\alpha = 90°$

an upside-down manner. Therefore, it can be concluded that a self-organized boundary layer suction and blowing would be realized alternatively without any external energy input. It is noteworthy that at $\alpha = 75°$, a similar phenomenon could also be observed as that shown in Fig. 4g.

A fast Fourier transform analysis was performed to plot the frequency spectra of the measured dynamic lift forces acting on the test model at $\alpha = 90°$ and the result is illustrated in Fig. 16. The peak frequency was identified as 31.2 Hz, which was very much close to the vortex shedding frequency from a natural cylinder (see Fig. 9). In addition, the corresponding period, T, was calculated to be 0.032 s. Since the sampling frequency of the pressure measurement was 312.5 Hz for the date acquisition, which was about ten times the target signals, it was possible to capture the time-variant pressure distributions on the cylinder surface. The obtained time-variant pressure data have been non-dimensionalized by Eq. (1), and the instantaneous distributions of the surface pressure coefficients within one period were plotted (Fig. 17).

As shown in Fig. 17, the negative pressure near the upper end (i.e., $\theta = 90°$) was found to be large at $t = 0$, and the pressure difference between the two slot ends were notably high. The pressure difference would drive a boundary layer suction. Consequently, the point of flow separation was delayed on the upper end of the slot. A flow that could withstand adverse pressure gradient was observed closely adhered onto the cylinder wall and was moving along the surface of the suction side, as shown in Fig. 15a. Because the slot was a zero-net-mass flux (ZNMF) actuator, the suctioned airflow was evacuated simultaneously through the lower end of the slot. With the change of time (t), the pressure distributions were found to fluctuate greatly. From the pressure distributions, it can be predicted that the suction would be gradually weakened on the upper end since the negative pressure region recovered gradually. When the time increased to the half-period ($t = 0.5$ T), the large negative pressure distribution was formed near $\theta = 270°$, indicating that the suction side had been shifted to the lower end, while the upper slot end worked as the blowing end. At this time, the distribution of surface pressure coefficients was found to be symmetric with that of $t = 0$ at about $\theta = 180°$. It corresponded to the instantaneous flow structures plotted in Fig. 15b. The great pressure fluctuations on the cylinder surface would also result in larger aerodynamic forces acting on the cylindrical model. As time continued to increase to a whole period ($t = T$), the pressure distributions were found to exhibit similarity to $t = 0$. Presumably, the boundary layer suction would occur at the upper end again. Therefore, the periodically fluctuating pressure distributions on the cylinder

surface would lead to an alternative boundary layer suction and blowing process on both ends of the slot at $\alpha = 90°$. The alternating frequency was found to be consistent with the vortex shedding frequency.

4 Concluding remarks

The flow characteristics around a circular cylinder with a slot at different angles of attack were experimentally investigated in the present study. The cylindrical test model was manufactured with a slot having a fixed slot width of $S = 0.075\ D$ and viable angle of attack α (i.e., changing from 0° to 90°). The experimental study was performed in a wind tunnel at the Reynolds number of $Re = 2.67 \times 10^4$ based on the cylinder diameter and the speed of incoming airflow. The pressure distribution measurements on the cylinder surface and PIV measurements were both conducted to quantify the flow around the natural and slotted cylinders at various angles of attack.

At low angles of attack ($\alpha = 0°$–$30°$), the slot was found to contribute to a passive flow control scheme. As a result, both C_D and C_L of the slotted cylinder were found to be lower than the baseline values, and the wake flow patterns were modified greatly. For the test case with slot at the angle of attack $\alpha = 0°$, it can be observed from the PIV measurement results that the passive flow generated from the slot would jet into the near wake and interact with the recirculating flow behind the cylinder, resulting in two recirculation regions in the wake behind the test model. A linear stability analysis was also conducted to confirm the vortex formation behind the slot cylinder. A bistable flow phenomenon, which is often referred to as flip-flop, was also identified and discussed for the test case with the slot at $\alpha = 0°$.

When the angle of attack of the slot reached 45°, the effects of the slot were found to be minimal and almost negligible. The surface pressure distributions, aerodynamic coefficients and wake flow patterns behind the slotted cylinder for this test case were found to exhibit significant similarity to the natural cylinder without slot (i.e., the baseline case).

As the angle of attack of the slot continued to increase (i.e., $\alpha = 60°$–$90°$), self-organized boundary layer suction and blowing without requiring any external energy input were observed. For the angle of attack of the slot 90°, instantaneous flow structures behind the slotted cylinder revealed that a boundary layer suction was performed on one end of the slot and the flow separation point from this side was substantially delayed. A vortex was formed and closely adhered onto the cylinder wall and was moving along the surface of the suction side, while another strong vortex was found to form and grow on the other end. Pressure measurement results revealed that the pressure difference between the two ends would lead to a boundary layer suction. Furthermore, the periodically fluctuating and changing pressure distributions were found to be responsible for the alternative boundary layer suction and blowing process on both ends of the slot as well as the larger aerodynamic forces acting on the slotted cylindrical model. Due to the alternative boundary layer suction and blowing, the flow separation points on both sides were found to be notably delayed, the wake width behind the slotted cylinder was decreased and the vortex formation length was greatly shrunk, in comparison to the baseline case for the cylinder without slot.

The findings of the present study also imply that, for a certain passive flow control method, the effectiveness of the flow control could be decreased greatly and even be switched to negative effects under different experimental settings (i.e., the slot at different directions in relation to the incoming flow for the present study). Further extensive studies are still needed to elucidate the underlying physics and to examine the relevant parameters, such as the possible flow directions and other important flow parameters, to explore/optimize the design paradigms in the implementation of a passive flow control scheme to various practical engineering applications.

Acknowledgements This work was funded by the National Natural Science Foundation of China through Grants 51378153, 51578188, 51008093 and 51161120359, and the Fundamental Research Funds for the Central Universities (HIT. BRETIII. 201512), and is also supported by the Opening Funds of the State Key Laboratory of Building Safety and Built Environment.

References

Adrian R, Christensen K, Liu ZC (2000) Analysis and interpretation of instantaneous turbulent velocity fields. Exp Fluids 29:275

Anderson E, Szewczyk A (1997) Effects of a splitter plate on the near wake of a circular cylinder in 2 and 3-dimensional flow configurations. Exp Fluids 23:161–174

Antonia R, Zhu Y, Sokolov M (1995) Effect of concentrated wall suction on a turbulent boundary layer. Phys Fluids 7(10):2465–2474

Baek H, Karniadakis GE (2009) Suppressing vortex-induced vibrations via passive means. J Fluids Struct 25(5):848

Barlow B, Rae H, Pope A (1999) Low-speed wind tunnel testing, 3rd edn. Wiley, New York, pp 330–375

Bearman PW (1965) Investigation of the flow behind a two-dimensional model with a blunt trailing edge and fitted with splitter plates. J Fluid Mech 21:241–255

Bearman PW, Wadcock AJ (1973) The interaction between a pair of circular cylinders normal to a stream. J Fluid Mech 61:499

Benard N, Balcon N, Touchard G, Moreau E (2008) Control of diffuser jet flow: turbulent kinetic energy and jet spreading enhancements assisted by a non-thermal plasma discharge. Exp Fluids 45:333–355

Brika D, Laneville A (1993) Vortex-induced vibrations of a long flexible circular cylinder. J Fluid Mech 250:481

Chen WL, Li H, Hu H (2014) An experimental study on a suction flow control method to reduce the unsteadiness of the wind loads acting on a circular cylinder. Exp Fluids 55(4):1–20

Chen WL, Gao DL, Yuan WY, Li H, Hu H (2015) Passive jet control of flow around a circular cylinder. Exp Fluids 56(11):201
Chew YT, Cheng M, Luo SC (1995) A numerical study of flow past a rotating circular cylinder using a hybrid vortex scheme. J Fluid Mech 299:35
Choi J, Jeon W-P, Choi H (2006) Mechanism of drag reduction by dimples on a sphere. Phys Fluids 18:041702
Choi H, Jeon WP, Kim J (2008) Control of flow over a bluff body. Annu Rev Fluid Mech 40:113–139
Degani AT, Walker JD, Smith FT (1998) Unsteady separation past moving surfaces. J Fluid Mech 375:1
Dong S, Triantafyllou GS, Karniadakis GE (2008) Elimination of vortex streets in bluff-body flows. Phys Rev Lett 100(20):204501
Gao DL, Chen WL, Li H, Hu H (2017) Flow around a circular cylinder with slit. Exp Thermal Fluid Sci 82:287–301
Gran RL, Lewis JE, Kubota T (1974) The effect of wall cooling on a compressible turbulent boundary layer. J Fluid Mech 66(03):507–528
Hwang J-Y, Yang K-S, Sun S-H (2003) Reduction of flow-induced forces on a circular cylinder using a detached splitter plate. Phys Fluids 15:2433–2436
Irwin H, Cooper R, Girard R (1979) Correction of distortion effects caused by tubing systems in measurements of fluctuating pressures [J]. J Wind Eng Ind Aerodyn 5(1):93–107
Joslin RD (1998) Aircraft laminar flow control. Annu Rev Fluid Mech 30(1):1–29
Kang S (2003) Characteristics of flow over two circular cylinders in a side-by-side arrangement at low Reynolds numbers. Phys Fluids 15(9):2486
Kim HJ, Durbin PA (1988) Investigation of the flow between a pair of circular cylinders in the flopping regime. J Fluid Mech 196:431
MacManus DG, Eaton JA (2000) Flow physics of discrete boundary layer suction–measurements and predictions. J Fluid Mech 417:47–75
Meyer KE, Pedersen JM, Özcan O (2007) A turbulent jet in crossflow analysed with proper orthogonal decomposition. J Fluid Mech 583:199–227
Mittal S, Kumar B (2003) Flow past a rotating cylinder. J Fluid Mech 476(4):303
Orszag SA (1971) Accurate solution of the Orr-Sommerfeld stability equation. J Fluid Mech 50(4):689
Owen JC, Bearman PW, Szewczyk AA (2001) Passive control of VIV with drag reduction. J Fluids Struct 15:597–605
Piomelli U, Balaras E, Pascarelli A (2000) Turbulent structures in accelerating boundary layers. J Turbul 1(1):01
Rodriguez O (1991) Base drag reduction by the control of three-dimensional unsteady vortical structures. Exp Fluids 11:218–226
Roshko A (1993) Perspectives on bluff body aerodynamics. J Wind Eng Ind Aerodyn 49(1-3):79
Schlichting H, Gersten K, Krause E (1979) Boundary-layer theory [M]. McGraw-hill, New York, pp 379–402
Sirovich L (1987) Turbulence and the dynamics of coherent structures. Part I: coherent structures. Q Appl Math 45(3):561–571
Tombazis N, Bearman PW (1997) A study of three-dimensional aspects of vortex shedding from a bluff body with a mild geometric disturbance. J Fluid Mech 330:85–112
Triantafyllou G, Triantafyllou M, Chryssostomidis C (1986) On the formation of vortex streets behind stationary cylinders. J Fluid Mech 170:461–477
Wang C, Tang H, Yu SC, Duan F (2016) Active control of vortex-induced vibrations of a circular cylinder using windward-suction-leeward-blowing actuation. Phys Fluids 28(5):053601
Williamson CHK (1985) Evolution of a single wake behind a pair of bluff bodies. J Fluid Mech 159:1
Zdravkovich MM (1981) Review and classification of various aerodynamic and hydrodynamic means for suppressing vortex shedding. J Wind Eng Ind Aerodyn 7:145–189
Zhou Y, Zhang HJ, Yiu MW (2002) The turbulent wake of two side-by-side circular cylinders. J Fluid Mech 458:303
Zhou B, Wang X, Guo W, Gho WM, Tan SK (2015) Control of flow past a dimpled circular cylinder. Exp Thermal Fluid Sci 69:19–26